

# Microstructure and mechanical properties of Ti/W and Ti–6Al–4V/W composites fabricated by powder-metallurgy

M. Frary<sup>a</sup>, S. Abkowitz<sup>b</sup>, S.M. Abkowitz<sup>b</sup>, D.C. Dunand<sup>a,\*</sup>

<sup>a</sup> Department of Materials Science and Engineering, Northwestern University, 2225 North Campus Drive, Evanston, IL 60208, USA

<sup>b</sup> Dynamet Technology Inc., Eight A Street, Burlington, MA 01803, USA

Received 19 February 2002; received in revised form 21 May 2002

## Abstract

Tungsten-reinforced Ti and Ti–6Al–4V composites were fabricated by powder metallurgical techniques from Ti, W and Al–V powders. The microstructure of the composites consists of partially dissolved tungsten particles within an  $\alpha/\beta$  titanium matrix containing tungsten in solid-solution. Yield and ultimate tensile strengths increase linearly with tungsten content in the range 0–15 wt.% W and decrease near-linearly with temperature in the range 25–540 °C. Ductility follows the opposite trend and is within technologically acceptable values, except for Ti/15W at 315 and 425 °C and Ti/10W at 540 °C which fractured near the ultimate stress value. The Ti–6Al–4V/10W composite shows the best combination of high strength and ductility at all temperatures. At ambient temperatures, Ti/10W exhibits a stress–strain curve very similar to Ti–6Al–4V (with a slight decrease in stiffness), while eliminating aluminum and vanadium alloy elements. Further improvements in mechanical properties of these non-equilibrium composites are likely to be achieved through optimized heat-treatments, which affect the matrix microstructure and the degree of dissolution of tungsten and thus the relative importance of matrix solid-solution strengthening and composite strengthening.

© 2002 Published by Elsevier Science B.V.

*Keywords:* Ti/W and Ti–6Al–4V/W composites; Powder-metallurgy; Mechanical properties

## 1. Introduction

The choice of reinforcing phases in titanium-matrix composites is severely limited by titanium's high reactivity with most ceramics and its high solubility for oxygen and nitrogen. Only a few ceramic reinforcements are thermodynamically stable with titanium and Ti–6Al–4V. Of these stable ceramics, the main representative is titanium carbide (we use TiC in the following, but  $\text{TiC}_{1-x}$  would be more accurate, given the large stoichiometric range [1,2]): TiC has been used in titanium and titanium alloys as particulate reinforcement [2–8] or formed in-situ during reaction with carbon [9], often as coating on SiC fibers [10]. TiB is another main phase thermodynamically stable with titanium, and can be formed in-situ following high-temperature dissolution of  $\text{TiB}_2$  [7,8,11] or other B-

containing materials [12]. Among metals, vanadium, molybdenum and tungsten stand out as potential reinforcements in titanium, because of their low solubility in  $\alpha$ -Ti (3 wt.% for V and 0.8 wt.% for Mo and W) and the lack of any intermetallic compounds with titanium [1]. Above the allotropic temperature of titanium (882 °C), all three transition metals, however, show complete solubility with  $\beta$ -Ti; these solid-solution alloys transform eutectoidally on cooling into  $\alpha$ -Ti and the pure transition metal [1]. Thus, below the eutectoid temperature, a composite consisting of a titanium matrix and vanadium, molybdenum or tungsten reinforcement is thermodynamically stable, i.e. there is no compound formation and only very limited interdiffusion between the phases. The eutectoid temperatures are 675 °C for Ti–V, 695 °C for Ti–Mo, and 740 °C for Ti–W [1], and thus exceed by far the upper potential use temperatures of these alloys, which is limited by oxidation of titanium. Among these three metals, tungsten is particularly attractive as reinforcement for titanium, as it has high stiffness, strength and density-compensated

\* Corresponding author. Tel.: +1-847-491-5370; fax: +1-847-467-6573

E-mail address: [dunand@northwestern.edu](mailto:dunand@northwestern.edu) (D.C. Dunand).

strength. Also, because of its very high melting point, tungsten is expected to show the slowest dissolution and diffusion kinetics in  $\beta$ -Ti, if a short processing temperature excursion is needed above the eutectoid temperature.

In the present paper, we investigate the fabrication of Ti/W and Ti–6Al–4V/W composites by powder-metalurgy methods minimizing time at high-temperature where dissolution can take place. We further study the microstructure of these composites and their mechanical properties, both at ambient and elevated temperatures.

## 2. Materials and experimental procedures

The average tungsten powder size (Fisher Sub-Sieve Size) is 3  $\mu\text{m}$ , but powders as large as 10  $\mu\text{m}$  were present. The titanium powders are roughly shaped, with an aspect ratio of about 2; they were sieved to less than 150  $\mu\text{m}$  and had an approximate size of 125  $\mu\text{m}$ . Their oxygen content was approximately 0.25 wt.%. For Ti–6Al–4V specimens, Al–V master alloy powders with size below 50  $\mu\text{m}$  were used.

Materials were processed by the combined cold and hot isostatic pressing (CHIP) technology [7]. Powders were compacted into green billets by cold-isostatic pressing at a pressure of 379 MPa. The billets were then vacuum-sintered at 1230  $^{\circ}\text{C}$  for 2.5 or 4 h and finally subjected to hot-isostatic pressing (HIP) at 900  $^{\circ}\text{C}$  for 2 h at 100 MPa, terminated by accelerated argon-cooling to room temperature in approximately 45 min. Two matrices (unalloyed titanium and Ti–6Al–4V) and three tungsten contents (0, 10 and 15 wt.% or 0, 2.8 and 4.4 at.%) were explored, corresponding to a total of six alloys labeled as Ti, Ti/10W, Ti/15W and Ti–6Al–4V, Ti–6Al–4V/10W, Ti–6Al–4V/15W. A summary of sintering times and post-processing densities (averaged over ten separate billets for each material) is given in Table 1 for all six materials.

Metallographic sample preparation consisted of grinding on SiC paper, polishing with diamond and alumina slurries, and etching with a modified Kroll's reagent (5% nitric acid, 10% HF, 85% water). All scanning electron microscopy (SEM) characterization

was performed on a Hitachi S-3500 instrument at an accelerating voltage of 15 kV, using imaging by secondary and back-scattered electrons, and energy-dispersive spectrometry (EDS), with a spot size of 15 nm.

Vickers hardness was measured on polished sections at ambient temperature, with a load of 200 g and an indent time of 10 s. Tensile tests at ambient temperature were performed on one specimen of each material, machined to ASTM E-8 proportional standards with a 34 mm gauge length and 6.4 mm gauge diameter. The cross-head speed was 12.7 mm  $\text{min}^{-1}$ , corresponding to an initial strain rate of  $6.2 \times 10^{-3} \text{ s}^{-1}$ . The strain was measured with an extensometer (with 25.4 mm gauge length) as well as with cross-head displacement.

High-temperature tensile tests were performed on specimens with the same dimensions as for ambient-temperature testing. Tests were conducted at 315, 425 and 540  $^{\circ}\text{C}$  under argon atmosphere. Each specimen was heated in about 30 min to the test temperature and soaked for 10 min before performing the test at a constant cross-head speed of 2.54 mm  $\text{s}^{-1}$ , corresponding to an initial strain rate of  $7.5 \times 10^{-2} \text{ s}^{-1}$ . The strain was measured by a water-cooled extensometer with an approximate gage length of 10 mm, and all tests were performed to fracture on a single specimen for each temperature.

Room- and elevated-temperature stiffness measurements were carried out in air by the frequency resonance technique using a GrindoSonic tester. Tests were conducted at the same four temperatures (25, 315, 425 and 540  $^{\circ}\text{C}$ ) with no soaking on all materials. Furthermore, Ti–6Al–4V/10W was annealed in air at 425  $^{\circ}\text{C}$  for 24 h and tested upon subsequent cooling to ambient temperature.

## 3. Results

### 3.1. Microstructure

Table 1 shows that little porosity exists in the densified materials. Negative porosity values may be due to small variations in tungsten content in the

Table 1  
Processing variables and initial conditions

Material	Sinter time (h)	Theoretical density ( $\text{g cm}^{-3}$ ) <sup>a</sup>	Initial density ( $\text{g cm}^{-3}$ )	Porosity (%) <sup>a</sup>
Ti	2.5	4.51	4.485	0.56
Ti/10 wt.% W	4	4.88	4.90	–0.40
Ti/15 wt.% W	4	5.09	4.99	1.96
Ti–6Al–4V	2.5	4.43	4.44	–0.23
Ti–6Al–4V/10 wt.% W	2.5	4.80	4.82	–0.42
Ti–6Al–4V/15 wt.% W	2.5	5.01	5.03	–0.40

<sup>a</sup> Assuming no chemical reaction.

preforms and/or formation of denser intermetallic phases with aluminum.

As expected, the Ti–6Al–4V sample shows complete dissolution of the Al–V master alloy powders and a microstructure typical of slow-cooled Ti–6Al–4V. All composites exhibit a matrix with a two-phase, Widmanstätten  $\alpha/\beta$  structure, as illustrated in Fig. 1 for Ti–6Al–4V/10W. The composition of each phase as measured by EDS was found to be W- and V-poor for the minority  $\alpha$ -phase and W-rich for the majority  $\beta$ -phase (Table 2).

Fig. 1 reveals that the tungsten powder particles consist of agglomerates of fine W particulates, as also confirmed by SEM observation of as-received powders. The interstices between the particulates are filled with titanium matrix. An unetched matrix region with high tungsten content surrounds each tungsten particle, suggestive of a diffusion zone. Fig. 1 shows such a W-rich diffusion zone,  $\sim 25 \mu\text{m}$  thick, around a  $\sim 50 \mu\text{m}$  diameter tungsten region which consists of individual tungsten particulates  $\sim 5 \mu\text{m}$  in size. As illustrated in Fig. 2a and b for Ti–6Al–4V/10W and Ti/10W, EDS composition profiles, measured from the center of the particle through the diffusion zone and into the matrix show that the tungsten content decreases monotonically from 40 wt.% W (within particle center) to 15 wt.% W (within matrix far from particle).

### 3.2. Mechanical properties at ambient temperature

As shown in Fig. 3, significant increases in hardness result from alloying titanium with tungsten, i.e. a near doubling in hardness between Ti (211 HV) and Ti/15W (372 HV). A 10 wt.% tungsten addition to Ti–6Al–4V also increases hardness from 339 HV to 408 HV, but there is no further improvement upon increasing the tungsten content to 15 wt.%.

Fig. 4 shows the stress–strain curves for all materials: strain hardening occurs shortly after the yield stress, and considerable necking is evident from the strain accumulated after the ultimate tensile stress, except for Ti–6Al–

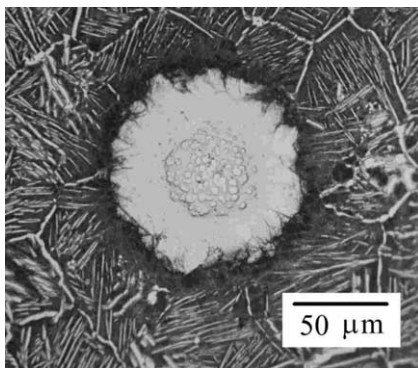


Fig. 1. Optical micrograph of Ti–6Al–4V/10W showing tungsten particle (consisting of multiple individual particulates), surrounded by unetched matrix shell with high W-content (white) and etched matrix.

4V/15W. Figs. 5 and 6 show the effect of tungsten content upon strength (yield and tensile stress) and ductility (failure strain and reduction in area), respectively. Yield stress increases sharply upon addition of tungsten to unalloyed titanium, e.g. by 87% from Ti to Ti/10W and by 149% from Ti to Ti/15W. The density increases are only 9 and 11%, respectively. Similar strength increments are achieved for Ti–6Al–4V. As expected from the strength increase, ductility decreases with increasing tungsten content, but remains within acceptable engineering values even for the strongest composites.

Finally, Fig. 7 shows that the Young's modulus at ambient temperature decreases with increasing tungsten content for both Ti and for Ti–6Al–4V. Also shown for Ti–6Al–4V/10W in Fig. 7 is the effect upon the Young's modulus of a 24 h. annealing treatment at 425 °C: the ambient temperature modulus increases by 12.5 GPa as compared with the untreated state, and rises above the

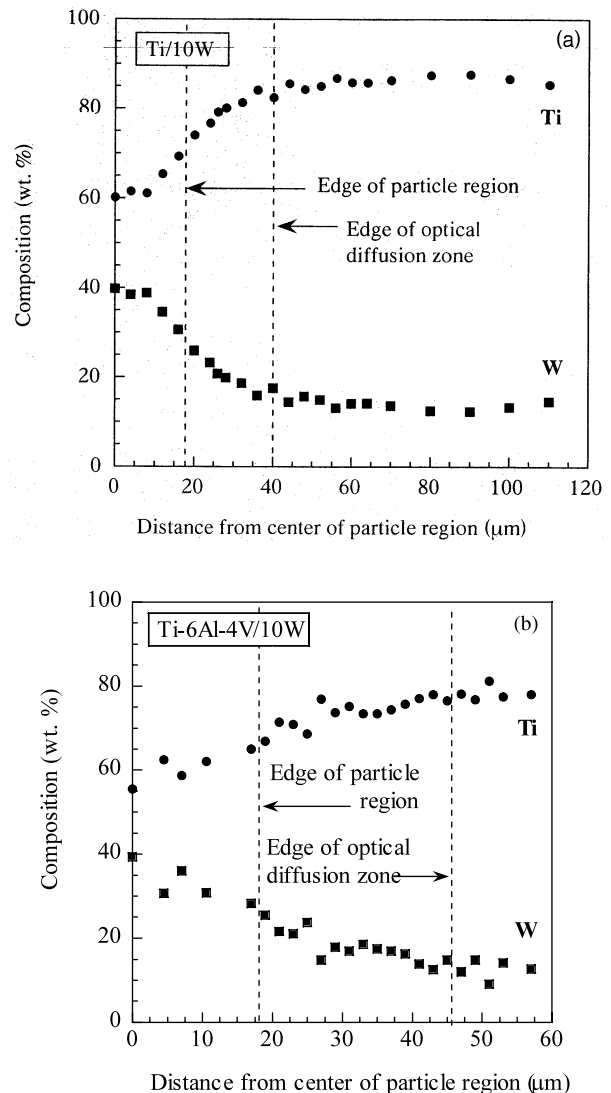


Fig. 2. Composition profile for (a) Ti/10W and (b) Ti–6Al–4V/10W.

Table 2  
Chemical composition (wt.%) of each phase as determined by EDS

	Ti/10W ( $\alpha$ -phase)	Ti/10W ( $\beta$ -phase)	Ti/15W ( $\alpha$ -phase)	Ti/15W ( $\beta$ -phase)	Ti–6Al–4V/ 10W ( $\alpha$ -phase)	Ti–6Al–4V/10W ( $\beta$ -phase)	Ti–6Al–4V/15W ( $\alpha$ -phase)	Ti–6Al–4V/15W ( $\beta$ -phase)
Ti	98.4 $\pm$ 1.1	90.4 $\pm$ 1.2	<sup>a</sup>	88.0 $\pm$ 0.8	90.0 $\pm$ 1.0	80.0 $\pm$ 1.3	89.6 $\pm$ 1.4	76.9 $\pm$ 1.1
Al	–	–	–	–	6.0 $\pm$ 0.8	4.0 $\pm$ 0.5	5.3 $\pm$ 0.3	3.8 $\pm$ 0.1
V	–	–	–	–	1.5 $\pm$ 0.3	5.0 $\pm$ 1.1	1.5 $\pm$ 0.4	3.6 $\pm$ 0.3
W	1.6 $\pm$ 1.1	9.6 $\pm$ 1.2	<sup>a</sup>	12.0 $\pm$ 0.8	2.5 $\pm$ 0.8	11.0 $\pm$ 1.0	3.6 $\pm$ 1.3	15.7 $\pm$ 1.2

<sup>a</sup> Unable to determine from specimen.

value of Ti–6Al–4V. A control experiment on Ti–6Al–4V heat-treated under the same conditions showed a much smaller increase in ambient temperature modulus (less than 2 GPa, within the estimated experimental error of 3 GPa).

### 3.3. Mechanical properties at elevated temperature

Fig. 8 shows the dependence on tungsten content of strength at 315 °C. As for ambient temperature, tungsten is found to very significantly strengthen both matrices, with a concomitant decrease in ductility. This decrease is relatively modest, with the exception of Ti/15W, which fractured in a brittle manner upon reaching the tensile strength value. Fig. 9 gives the strength at 425 °C as a function of tungsten content, showing the same general trends as at 315 °C. As for the tests at 315 °C, the Ti–15W sample fractured at the shoulder. Fig. 10 illustrates the stress–strain curves for each test at 540 °C. The Ti/15W now shows significant deformation beyond the ultimate tensile stress, while the Ti/10W fractured in a brittle manner at the shoulder near that value. Fig. 11 displays strength at 540 °C as a function of tungsten content. Finally, Fig. 7a and b show that the high-temperature stiffness of the Ti– and Ti–6Al–4V composites vary very little with tungsten content, unlike stiffness at ambient temperature. Fig. 7b further shows that Ti–6Al–4V/10W annealed for 24 h at 425 °C exhibits an increase in stiffness at 425 and 540 °C; the magnitude of this effect is, however, smaller than at room temperature.

The mechanical data are shown graphically as a function of temperature in Figs. 12 and 13 for strength and Figs. 14 and 15 for ductility. Low ductility values for Ti/15W at 315 °C and Ti/10W at 540 °C are due to premature fracture at the sample shoulders, possibly due to a small machining flaw.

## 4. Discussion

### 4.1. Microstructure

Metallographic analysis reveals partially-dissolved tungsten particles within a matrix with large quantities of tungsten in solid-solution. The matrix shows a Widmanstätten  $\alpha$ – $\beta$  structure, typical of slow cooling from the  $\beta$ -phase field. As expected,  $\alpha$  needles are depleted in tungsten and the  $\beta$ -matrix is enriched in tungsten. A similar, but opposite, effect was reported in the Ti-6242 alloy (Ti–6Al–2Sn–4Zr–2Mo) where molybdenum was segregated in the  $\alpha$  needles of the Widmanstätten structure [13]. As for many titanium alloys with other transition metal elements, a martensitic structure leading to a range of non-equilibrium phases is possible on rapid cooling, with an attendant change in

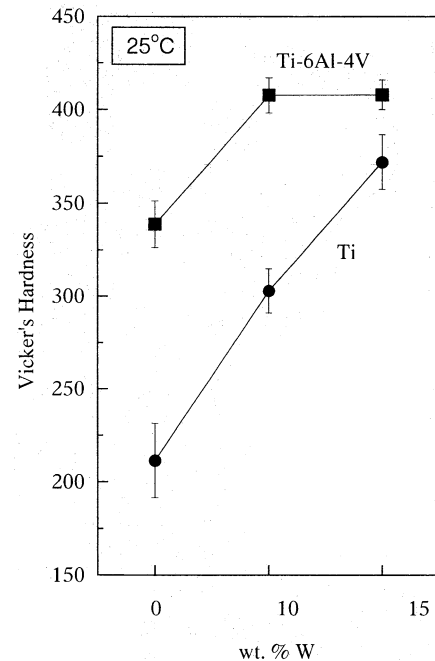


Fig. 3. Composition dependence of Vickers hardness at ambient temperature.

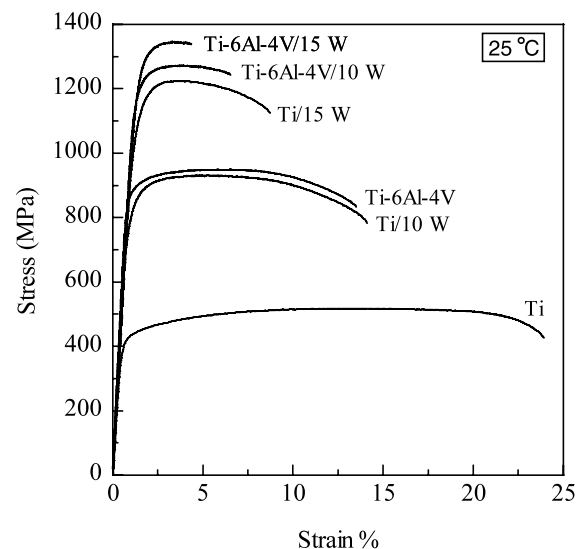


Fig. 4. Stress–strain curves at ambient temperature.

mechanical properties [13]. The average composition of the matrices of both Ti and Ti–6Al–4V composites is close to the equilibrium concentration of the alloy (Table 2), indicating that long-range diffusion of tungsten into the matrix occurred during processing. Concentration gradients near the tungsten particles (Fig. 2a–b), however, indicate that diffusion was not complete and that the microstructure is not at equilibrium. The titanium measured within the tungsten particles (Fig. 2a–b) is most probably not in solid-solution, but rather consists of tungsten-saturated titanium squeezed

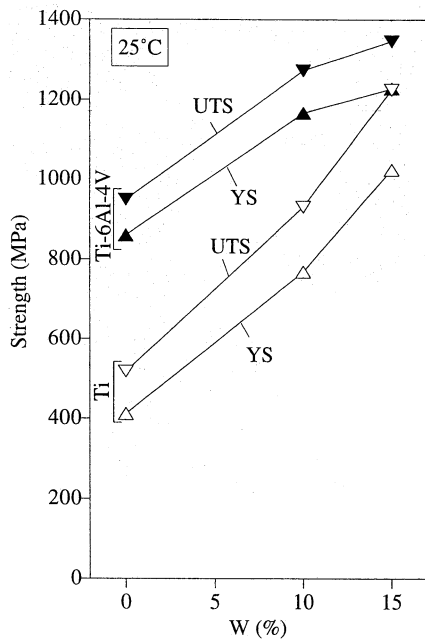


Fig. 5. Composition dependence of yield and ultimate tensile stress at ambient temperature.

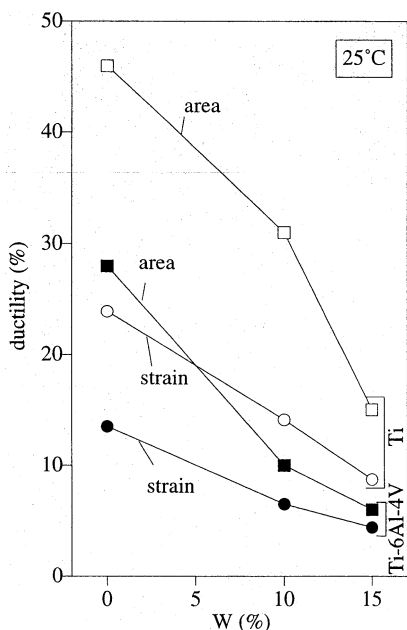


Fig. 6. Composition dependence of failure strain and reduction in area at ambient temperature.

by the high isostatic processing pressure within the interstices of the tungsten particles, as shown in Fig. 1.

The properties of the composites are thus expected to be controlled both by the solid-solution matrix and the tungsten particles. Furthermore, heat-treatment or high-temperature use of these materials with non-equilibrium structures will lead to further dissolution of the tungsten particles with a concomitant evolution of the mechanical properties.

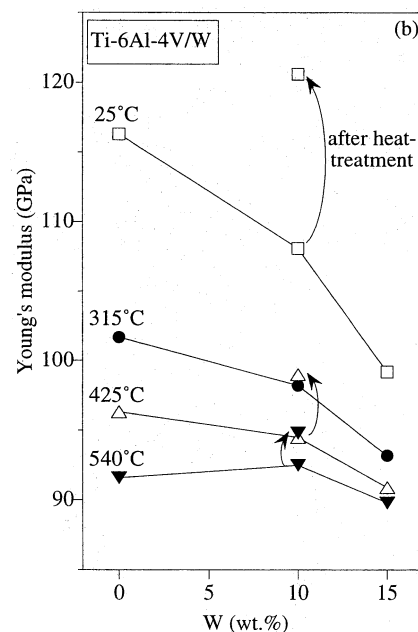
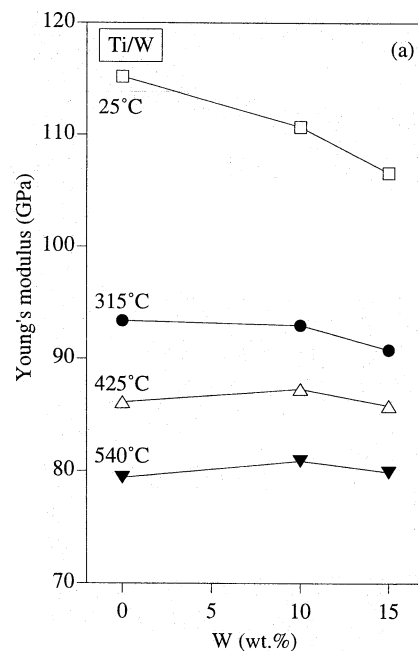


Fig. 7. Composition dependence of Young's modulus at ambient temperature for (a) Ti/W and (b) Ti-6Al-4V/W. Arrows mark evolution of stiffness after 24 h heat-treatment at 425 °C.

#### 4.2. Mechanical properties at ambient temperature

The powder-metallurgy Ti sample (with ca. 0.25 wt.% oxygen) has yield and tensile strengths higher than ASTM Grade 2 (with ca. 0.20 wt.% oxygen) and intermediate between those of ASTM Grades 3 and 4 unalloyed titanium (with ca. 0.35 and 0.40 wt.% oxygen, respectively [14]). Similarly, the powder-metallurgy Ti-6Al-4V sample (with ca. 0.28 wt.% oxygen) shows yield and tensile strengths significantly higher than Ti-6Al-

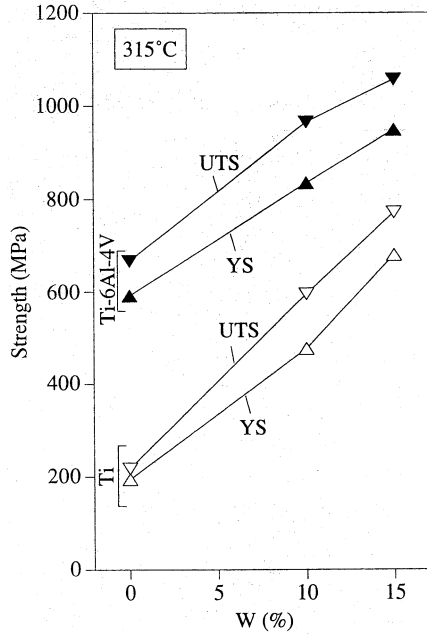


Fig. 8. Composition dependence of yield and ultimate tensile stress at 315 °C.

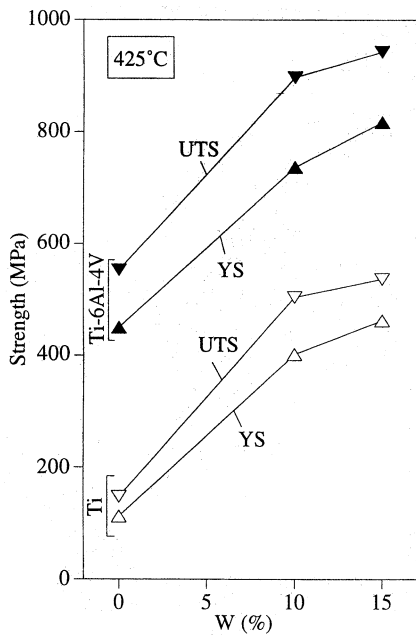


Fig. 9. Composition dependence of yield and ultimate tensile stress at 425 °C.

4V ELI (with less than 0.13 wt.% oxygen), and somewhat higher than yield and tensile strengths for wrought, annealed Ti-6Al-4V with approximately 0.20 wt.% oxygen (830 and 900 MPa, respectively); this is attributable largely to the higher oxygen content. Ductility values for both Ti and Ti-6Al-4V are well within the commercially-relevant range.

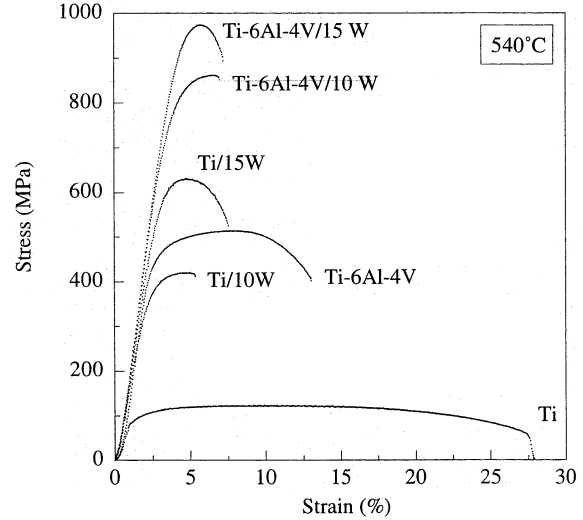


Fig. 10. Stress-strain curves at 540 °C.

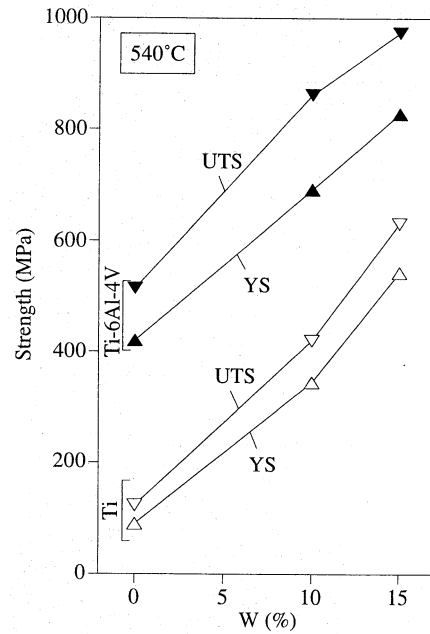


Fig. 11. Composition dependence of yield and ultimate tensile stress at 540 °C.

Figs. 4–6 show that tungsten is a potent strengthener in both Ti and Ti-6Al-4V. Typical strengthening of quenched  $\beta$ -alloys is 19–48 MPa per wt.% for the fourth period transition metals from V to Cu [13] and is comparable to the value found here for Ti-W in Fig. 5 (45 MPa per wt.% for the yield stress and 53 MPa per wt.% for the ultimate tensile stress). Direct comparison is not possible, as the Ti-W composites contain partially-dissolved tungsten, whose strengthening effect is thus divided between solid-solution (for the dissolved tungsten fraction) and load-transfer (for the undissolved tungsten fraction).

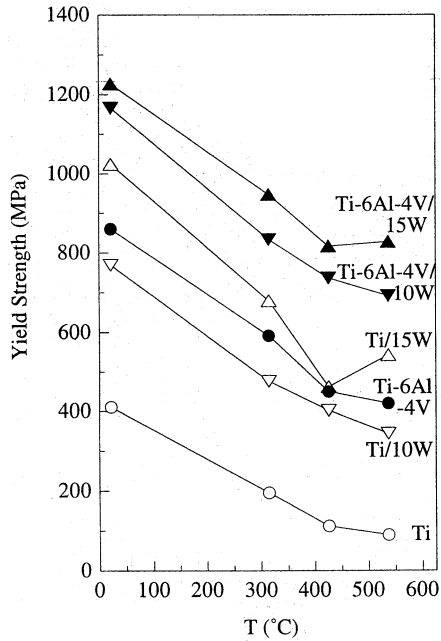


Fig. 12. Temperature dependence of yield stress.

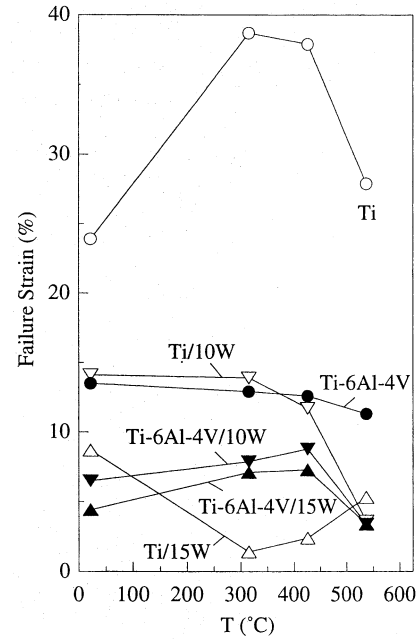


Fig. 14. Temperature dependence of failure strain.

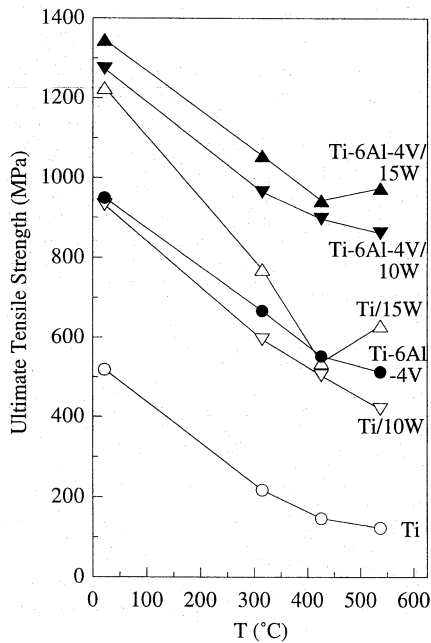


Fig. 13. Temperature dependence of ultimate tensile stress.

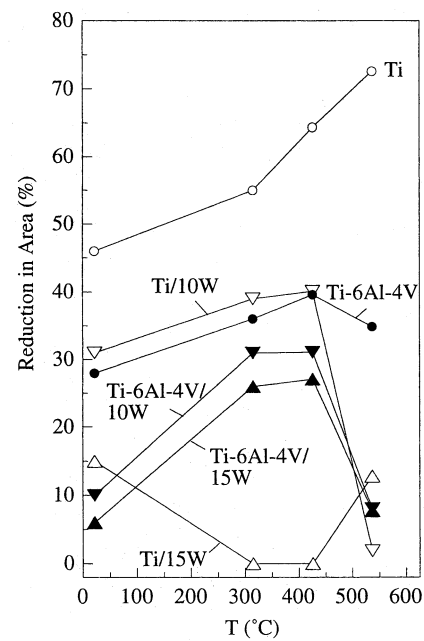


Fig. 15. Temperature dependence of area reduction.

As expected, ductility decreases with increasing strength, but failure strains are still exceptionally high given the very high strength levels. As compared with Ti and Ti-6Al-4V composites reinforced with TiC or TiB [2–8], the composites have much higher strength and ductility. In fact, Ti-6Al-4V/10W and Ti-6Al-4V/15W have mechanical properties approaching those of one of the strongest titanium alloys, Ti-5Al-2Sn-4Zr-4Mo-2Cr-1Fe (Beta-CEZ). Forged Beta-CEZ, after a

heat-treatment producing a ductility of 11% comparable to that of Ti-6Al-4V/10W, displays yield and ultimate tensile stress values of 1208 and 1283 MPa, which are very close (3 and 1% higher) to those of Ti-6Al-4V/10W. Similarly, after a heat-treatment producing a ductility of 5% (comparable to Ti-6Al-4V/15W), forged Beta-CEZ display strength values of 1304 and 1370 MPa, i.e. only 6 and 2% higher than Ti-6Al-4V/15W. We perform the above comparison using Beta-CEZ in its forged state (rather than in rolled or

'pancake' states), which is relevant to a near-net-shape object, as is the powder-metallurgy process for Ti–6Al–4V/W composites. It is noteworthy that Beta-CEZ is a highly-optimized alloy in terms of both composition and heat-treatment, while the present Ti–6Al–4V/W composites are un-optimized. Also noteworthy is the small difference in density between Beta-CEZ and Ti–6Al–4V/10W or Ti–6Al–4V/15W (2 and 7%, respectively).

Hardness measurements shown in Fig. 3 confirm the trends observed for the tensile strength (Fig. 5). For comparison, the hardness of tungsten is 350 HV in the annealed state and 440 HV in the work-hardened state [15]. The high hardness values of the composites are promising in applications which require good wear resistance, e.g. medical implants, boat propellers or automotive brakes, or for the matrix of composites containing hard ceramic particles [16].

Unlike strength, stiffness decreases with increasing tungsten content in both Ti and Ti–6Al–4V (Fig. 7a–b). This result clearly indicates that tungsten dissolves in the matrix and remains in solid-solution despite the modest cooling rate. There are three reasons for this conclusion. First, quenched  $\beta$ -alloys containing V, Nb and Mo in solid-solution exhibit a near linear decrease in stiffness with increasing alloying element content, with minima in the range of 70 GPa [13]. Second, elemental tungsten is much stiffer than titanium and should lead to marked increase in elastic modulus by load-transfer if it remains undissolved in the form of particles. The relatively small stiffness decrease as compared with the Ti–V, –Nb and –Mo alloys can be attributed to the partial dissolution of W, also observed metallographically (Fig. 1): tungsten in solution decreases the stiffness of the matrix, while the remaining undissolved tungsten stiffens the composite by load-transfer. Third, the marked increase in stiffness observed after a 24 h. anneal at 425 °C of Ti–6Al–4V/10W (Fig. 7b), has been observed in commercial  $\beta$ -alloys and in annealed Ti–Nb alloys, where it is explained by the evolution of non-equilibrium phases [13].

Somewhat fortuitously, the stress–strain curves of Ti–6Al–4V and Ti/10W are almost identical (Fig. 4). The latter material is free of aluminum and vanadium, which are suspected to be toxic when used as a biomaterial for implants or devices [17,18]. The modest increase in density (10%) is unimportant for biomedical applications, while the decrease in modulus is beneficial to reduce stress shielding in implants [19]. Also, increased radio-opacity provided by tungsten may be beneficial for very thin parts. Further tests (e.g. corrosion resistance as well as fatigue and fracture properties) will be necessary before Ti/10W can be considered as a replacement for Ti–6Al–4V for biomedical applications. Furthermore, most biomedical applications using Ti–6Al–4V require a maximum oxygen content of 0.13

wt.% (ELI grade), which lowers the ambient temperature strength to a level below that measured for Ti/10W.

#### 4.3. Mechanical properties at elevated temperature

The exceptional strengthening offered by tungsten additions at room temperature is maintained at elevated temperature, as illustrated in Figs. 8, 9 and 11. Except for Ti/15W at 315 and 425 °C and Ti/10W at 540 °C which fractured prematurely at the shoulders, the ductility of all composites is high enough for engineering application, while the strength is much improved as compared with unreinforced materials. Given for comparison in Table 3 are the strength and ductility values of two high-temperature titanium alloys, Ti–8Al–1Mo–1V in the rolled and annealed state and Ti-1100 (Ti–6Al–2.8Sn–4Zr–0.4Mo–0.5Si in the  $\beta$ -forged and annealed state) [20]. The strength of these two alloys is significantly less than that of Ti–6Al–4V/10W and Ti–6Al–4V/15W. Ductility is somewhat higher for the commercial alloys, except at 540 °C where the composite ductility drops to low values.

The mechanical data are shown graphically as a function of temperature in Figs. 12 and 13 for strength and Figs. 14 and 15 for ductility. Strength decreases monotonically with temperature, except for Ti/15W and Ti–6Al–4V/15W, which are stronger at 540 than at 425 °C. For the Ti/15W sample, this may be due to the anomalously low strength at 425 °C, with fracture occurring at the shoulder, possibly because of a flaw in the sample or a lack of densification during processing. On the other hand, the Ti–6Al–4V/15W sample seems stronger at 540 °C than expected based on the trend from ambient temperature to 425 °C. A possibility is that tungsten dissolved in the matrix during the heating and soaking period at 540 °C: the strengthening by solid-solution hardening is then higher than the weakening due to loss of tungsten particles. This indicates that further optimization of the mechanical properties can be achieved through heat-treatment, but also that 540 °C is too high a temperature for long-term use of the alloy. All composites show an increasing (or near constant) ductility between ambient temperature and 425 °C, followed by a sharp drop at 540 °C (except for Ti/15W whose ductility was very low at 315 and 425 °C). This again points to an upper use temperature below 540 °C.

## 5. Conclusions

Titanium or Ti–6Al–4V composites with 10 or 15 wt.% tungsten particles additions were compacted from powders at elevated temperature. Their microstructures consist of a  $\alpha/\beta$  Ti-matrix with tungsten in solid-

Table 3

Mechanical properties at elevated temperature for Ti–8Al–1Mo–1V (rolled and annealed) and Ti-1100 (Ti–6Al–2.8Sn–4Zr–0.4Mo–0.5Si,  $\beta$ -forged and annealed) [20]

	Yield stress (MPa)	Ultimate tensile stress (MPa)	Failure strain (%)	Area reduction (%)
<i>Ti–8Al–1Mo–1V</i>				
315 °C	586	779	11	23
425 °C	551	724	10	26
540 °C	503	655	14	30
<i>Ti-1100</i>				
315 °C	650	783	–	–
425 °C	640	750	–	–
540 °C	585	685	–	–

solution, containing partially-dissolved tungsten particles. Mechanical tests at ambient temperature and 315, 425 and 540 °C demonstrate that tungsten additions result in very significant improvements in yield and ultimate tensile strengths with an acceptable penalty in ductility (except for Ti/15W at 315 and 425 °C and Ti/10W at 540 °C). Ti–6Al–4V/10W is the best candidate in terms of high-strength applications at both ambient and elevated temperature, and has the potential to replace Ti–6Al–4V for some aerospace and industrial applications. At ambient temperatures, Ti/10W shows mechanical properties comparable to Ti–6Al–4V except for a slight decrease in stiffness. Ti/10W is thus a potential replacement for Ti–6Al–4V for cases where aluminum and vanadium alloy additions may be undesirable (e.g. in biomedical components). Further improvements in mechanical properties can be expected upon a systematic optimization of the alloying level and heat treatment. These parameters control both the matrix structure and the degree of dissolution of tungsten, which provides solid-solution strengthening when dissolved in the matrix and composite strengthening when undissolved.

### Acknowledgements

This research was supported through a SBIR grant from the National Science Foundation (#0060484). Useful discussions with W. Zimmer (AFML/ML) are acknowledged.

### References

- [1] ASM Handbook: Alloy Phase Diagrams, American Society for Metals, Metals Park, OH, 1992.
- [2] C. Badini, G. Ubertalli, D. Puppo, P. Fino, J. Mater. Sci. 35 (2000) 3903.
- [3] S. Abkowitz, P. Weihrauch, Adv. Mater. Proc. 136 (7) (1989) 31.
- [4] T.P. Johnson, J.W. Brooks, M.H. Loretto, Scr. Metall. Mater. 25 (1989) 785.
- [5] M.H. Loretto, D.G. Konitzer, Metall. Trans. 21A (1990) 1579.
- [6] M. Hagiwara, N. Arimoto, S. Emura, Y. Kawabe, H.G. Suzuki, Iron Steel Inst. Jpn. Int. 32 (1992) 909.
- [7] S. Abkowitz, P.F. Weihrauch, S.M. Abkowitz, Ind. Heat. 12 (1993) 32.
- [8] T.M.T. Godfrey, A. Wisbey, P.S. Goodwin, K. Bagnall, C.M. Ward-Close, Mater. Sci. Eng. A282 (2000) 240.
- [9] S.G. Warrior, R.Y. Lin, Scr. Metall. Mater. 29 (1993) 147.
- [10] C. Jones, C.J. Kiely, S.S. Wang, in: C.G. Pantano, E.J.H. Chen (Eds.), Interfaces in Composites, MRS, 1990, p. 179.
- [11] S.S. Sahay, K.S. Ravichandran, R. Atri, B. Chen, J. Rubin, J. Mater. Res. 14 (1999) 4214.
- [12] Z.Y. Ma, S.C. Tjong, L. Gen, Scr. Mater. 42 (2000) 367.
- [13] E.W. Collings, The Physical Metallurgy of Titanium Alloys, American Society for Metals, Metals Park, OH, 1984.
- [14] M.J. Donachie, Titanium—A Technical Guide, ASM, Metals Park, OH, 1988.
- [15] Metals Handbook: Properties and Selection: Nonferrous Alloys and Pure Metals, American Society for Metals, Metals Park, OH, 1979.
- [16] M.J. Koczak, S.C. Khatri, J.E. Allison, M.G. Bader, in: S. Suresh, A. Mortensen, A. Needleman (Eds.), Fundamentals of Metal Matrix Composites, Butterworth-Heinemann, Boston, MA, 1993, p. 297.
- [17] C.B. Johansson, T. Albrektsson, P. Thomsen, L. Senerby, A. Lodding, H. Odelius, Eur. J. Exp. Musculoskel. Res. 1 (1992) 161.
- [18] B.W. Callen, B.F. Lowenberg, S. Lugowski, R.N.S. Sodhi, J.E. Davies, J. Biomed. Mater. Res. 29 (1995) 279.
- [19] B.P. McNamara, A. Toni, D. Taylor, Adv. Eng. Mater. 99 (1995) 309.
- [20] R. Boyer, G. Welsch, E.W. Collings, Materials Properties Handbook: Titanium Alloys, ASM, Metals Park, OH, 1994.